Competition and Interhalogen Formation during Parallel Electrocatalytic Oxidation of Bromide and Chloride on Pt

Vos, Johannes G.; Venugopal, Anirudh; Smith, Wilson A.; Koper, Marc T.M.

DOI
10.1149/1945-7111/ab717c

Publication date
2020

Document Version
Final published version

Published in
Journal of the Electrochemical Society

Journal of The Electrochemical Society

Competition and Interhalogen Formation During Parallel Electrocatalytic Oxidation of Bromide and Chloride on Pt

Journal of The Electrochemical Society, 2020 **167** 046505

Competition and Interhalogen Formation During Parallel Electrocatalytic Oxidation of Bromide and Chloride on Pt

Johannes G. Vos,[1] Anirudh Venugopal,[2] Wilson A. Smith,[2] and Marc T. M. Koper[1,*,z]

[1]*Leiden Institute of Chemistry, Leiden University, 2300 RA Leiden, The Netherlands*
[2]*Materials for Energy Conversion and Storage (MECS), Department of Chemical Engineering, Delft University of Technology, 2629 HZ Delft, The Netherlands*

Hydrogen production from seawater electrolysis is highly promising for the capture and storage of intermittent renewable energy, but is hindered by the possibility of unwanted reactions at the anode. The oxidation reactions of chloride and (to a lesser extent) bromide, which can occur in parallel to the evolution of oxygen, lead to environmentally harmful by-products and thus represent undesirable side-reactions. We present some general considerations of solution chemistry and oxidation products that may be expected in a mixed acidic bromide/chloride electrolyte. We performed electrochemical model studies of the simultaneous oxidation of bromide and chloride and their mutual interaction on a Pt electrocatalyst, with the aim of deepening the general understanding of the anodic competition problem. Using simplified model systems, our findings suggest that the oxidation of bromide is hindered by competing chloride adsorption, in a way that can be quite satisfactorily modelled by a simple Langmuir isotherm describing the competing adsorption and reactivity of all species. The oxidation of chloride was however not properly captured by this same model, and may be substantially different. Furthermore, the formation of the interhalogen compound BrCl seems to occur in-between the oxidation of bromide and chloride.

 [DOI: 10.1149/1945-7111/ab717c]

Manuscript submitted October 21, 2019; revised manuscript received January 3, 2020. Published February 14, 2020.

Supplementary material for this article is available online

In a future energy infrastructure based on renewables, a major role is expected for water electrolysis.[1–3] In an electrolyser, the cathode produces the desired compound, such as H_2; an anodic reaction is needed to complete the electrochemical device. Usually, this reaction is the oxygen evolution reaction (OER), due to the benign nature of the O_2 formed. Furthermore, when water electrolysis is to be carried out on large scale, using seawater as feedstock would lessen the potential strain on precious freshwater resources; it would also offer a significant infrastructural advantage, since freshwater is generally scarce in areas where the influx of solar energy is the highest.[4,5] Unfortunately, the presence of chloride in seawater leads to a substantial risk of evolving chlorine on the anode,[6–8] which is a toxic and kinetically labile oxidizing agent. Due to an apparent scaling relationship between the OER and the chlorine evolution reaction (CER),[9–11] any OER-active anode has a propensity to form a mixture of oxygen and chlorine or oxygenated chloride species in a chloride-containing electrolyte. Additionally, seawater contains a small but significant amount of Br^-, roughly 0.3 mol% relative to chloride.[12] Analogous to the CER, bromide can rapidly be oxidized on the anode via the bromine evolution reaction (BER) and form corrosive products which are not easily disposed of in an environmentally friendly way. Oxidation of either Cl^- or Br^- always tends to compete with the formation of O_2, and these are therefore undesirable processes that are likely to happen during seawater electrolysis for energy storage. Oxidation of either Cl^- or Br^- is also an important consideration during the electrochemical treatment and disinfection of wastewater. Anodic formation of Cl_2 and especially Br_2 may result in halogenation of organic compounds present in the water, which is highly detrimental to the detoxification performance.[13–15] Finally, the BER also is relevant to the energy intensive chlor-alkali process, where Br^- is a common contaminant in the brine feedstock.[16]

The BER and CER have been studied individually in the past, where the CER has received by far the most attention in light of its industrial importance.[17] Much less research has gone into systems where both Cl^- and Br^- are present, such as when using seawater or a seawater-derived electrolyte, in which the BER and CER can occur simultaneously. To the best of our knowledge, the literature on this rather complex situation is scarce, and is mostly carried out from the perspective of wastewater treatment.[18–20] Our interest goes out specifically to the fundamental understanding of the parallel (i.e., simultaneous) halogen oxidation reactions, which can be beneficial to seawater electrolysis and water treatment alike. The BER and CER seem to follow similar electrocatalytic pathways,[21–24] which implies that the active sites involved in the reactions would be the same, and that some form of interaction between them can be expected. One could then imagine that the two reactions simply mutually inhibit each other, or form an intimate coupling that can lead to changes in the reaction pathway and the formation of interhalogen compounds. Either case can have important practical implications, since in the first case, one reaction may block the occurrence of the other one if the ratio between reactants is unbalanced enough; in the latter case, interaction between the two reactants can lead to unexpected outcomes.

In this paper, we explore the parallel oxidation of bromide and chloride on a Pt electrocatalyst, which exhibits significant electrocatalytic activity for both the CER and BER. As a simplified model system, we use solutions containing HCl and HBr in varying ratios with additional $HClO_4$ as background electrolyte, preventing the presence of cations in solution, which may have an influence on the kinetics.[25–27] The low pH was intended to prevent complications from the formation of oxygenated chlorine or bromine species (such as ClO^- or BrO_3^-), which is favored by high pH,[28,29] and also allowed to study both the BER and CER on Pt with minimal interference from the OER. We utilize forced convection studies using an rotating ring-disk electrode (RRDE) to gain insight into the kinetic competition and interdependence of the two reactions, coupled to a Pt ring that allows quantitative detection of soluble halogen products.[30] Special focus was on Tafel behavior and reaction orders as a function of potential and reactant concentration. Of especial interest were mutual inhibiting effects, and the possible electrochemical formation of interhalogen compounds, such as BrCl. Kinetic studies were complemented with in-situ electrochemical UV–vis experiments on stationary electrodes, to probe the formation of products as a function of potential and time near the electrode surface. The combination of these techniques sheds light on how

*Electrochemical Society Member.
[z]E-mail: m.koper@chem.leidenuniv.nl

chloride and bromide interact on a model electrocatalyst, and the implications this may have in a practical setting.

Experimental

All experiments were carried out at room temperature (~20 °C). Cleanliness protocols for the RRDE experiments were considerably more rigorous than those for the UV–vis experiments, because forced-convection techniques are inherently more sensitive to contamination.

Chemicals.—For the RRDE experiments, $HClO_4$ (70%, Suprapur®/Trace analysis grade) and HCl (30%, Ultrapur®/Trace analysis grade) were purchased from Merck. HBr (47%, Normapur®/Analysis grade) was purchased from VWR Chemicals. For the UV–vis experiments, $HClO_4$ (60%, EMSURE/Analysis grade), HCl (32%, EMSURE/Analysis grade) and HBr (47%, EMSURE/Analysis grade) were purchased from Merck. All purchased chemicals were used as received. The water used for all experiments was prepared by a Merck Millipore Milli-Q system (resistivity 18.2 MΩcm, TOC < 5 p.p.b.).

Cleaning procedures.—For the RRDE experiments, all glassware was thoroughly cleaned before first-time use by boiling in a 3:1 mixture of concentrated H_2SO_4 and HNO_3. When not in use, all glassware was stored in a 0.5 M H_2SO_4 solution containing 1 g l^{-1} $KMnO_4$. Before each RRDE experiment, glassware was thoroughly rinsed with water, and then submerged in a dilute (~0.01 M) solution of H_2SO_4 and H_2O_2 to remove all traces of $KMnO_4$ and MnO_2. The glassware was then rinsed three times with water and boiled in water. The rinsing-boiling procedure was repeated two more times.

The glassware and custom-built cell for UV–vis experiments were cleaned by soaking in warm reagent grade 98% H_2SO_4 for an hour, followed by copious rinsing with Milli-Q water and boiling three times in Milli-Q water. When not in use, they were stored submerged in Milli-Q water.

Electrode preparation.— *RRDE experiments.*—Pt disks of 5 mm diameter (0.196 cm^2 geometrical surface area) were used as primary working electrode, along with a Pt ring as secondary electrode. At the beginning of an experimental session, the assembled Pt-Pt tip was rinsed with copious amounts of Milli-Q water, treated for 3 min with a solution of 0.5 M H_2SO_4 containing 0.5 g l^{-1} $KMnO_4$, rinsed with Milli-Q water, treated with a dilute (~0.01 M) solution of H_2SO_4 and H_2O_2 to remove any traces of $KMnO_4$ and MnO_2, and then extensively rinsed with warm (~50 °C) Milli-Q water. During RRDE experiments, the Pt disk and ring electrodes were electropolished by scanning from −0.1 V to 1.7 V at 500 mV s^{-1} for 20 scans at 1500 RPM. In-between experiments, the disk electrode was kept at 0.7 V vs RHE. Ring currents were corrected for constant background currents and product collection delay. The latter arises from the time needed for products formed on the disk to reach the ring. The delay for each used rotation rate was empirically determined by stepping the potential to evolve Br_2 on the disk, and investigating the ring response as a function of time (Fig. S 3 is available online at stacks.iop.org/JES/167/046505/mmedia).

Before each experiment, the Pt electrode was subjected to a pretreatment step to ensure an oxide-free, reproducible surface (see Fig. S 1). The electrode was first kept at 0.4 V vs RHE for 10 s, to reduce any residual trace of platinum oxide of preceding experiments, followed by a 3 s hold at 0.7 V vs RHE, to equilibrate the electrode and allow capacitive double layer charging to minimize. Scanning commenced immediately afterwards.

UV–vis experiments.—A 5 nm platinum layer was sputtered onto a conductive fluorine doped tin oxide (FTO) substrate (TEC-15, Hartford glass co.), for the in-situ UV–vis transmission measurements. The deposition was performed at 3 μbar deposition pressure, with a deposition rate of ~0.593 Å s^{-1}, using an AJA sputtering system (ATC 2400). The FTO substrate was cleaned, prior to the deposition, using a sequence of laboratory soap, Milli-Q water, acetone and isopropanol and eventually drying the substrates with nitrogen gas. Subsequently, the FTO substrate surface was also cleaned using argon plasma for 2 min, prior to the platinum layer deposition.

Cell preparation.— *RRDE experiments.*—RRDE experiments were done with home-made two-compartment borosilicate glass cells with solution volumes of 100 ml. An IviumStat potentiostat (Ivium Technologies) run by the IviumSoft software package was used for potential control. All experiments were done with a MSR rotator and E6 ChangeDisk RRDE tips in a PEEK shroud (Pine Research). All experiments were 95% iR-compensated during the experiment, by measuring the solution resistance with electrochemical impedance spectroscopy at 0.70 V vs RHE, and observing the absolute impedance in the high frequency domain (100–50 KHz) corresponding to a zero-degree phase angle. All used solutions were saturated with Ar (Linde, purity 6.0) before experiments. During forced convection experiments, solutions were continuously bubbled with Ar gas. The reference electrode was a HydroFlex® reversible hydrogen electrode (Gaskatel), separated from the main solution using a Luggin capillary. An additional LowProfile Ag/AgCl reference electrode (Pine Research) served to measure the solution pH and was used for conversion to the NHE scale. The Ag/AgCl reference was externally calibrated on a regular basis and had a value of 198 ± 0.5 mV vs NHE. All potentials in this paper are reported on the NHE scale unless explicitly mentioned otherwise. A flame-annealed Pt mesh was used as counter electrode, separated from the main solution by a coarse sintered glass frit.

UV–vis experiments.—A Vertex potentiostat (Ivium Technologies) run by the IviumSoft software package was used for potential control. The transmission measurements were performed in a custom-built setup, consisting of a PTFE electrochemical cell housing equipped with quartz windows. A coiled platinum wire acted as the counter electrode, and a LowProfile Ag/AgCl reference electrode (Pine Research) was placed in fixed position relative to the Pt/FTO working electrode. The Ag/AgCl electrode was calibrated at 199 ± 0.5 mV vs NHE. All applied potentials were 90% iR-compensated according to the solution resistance. The latter was measured using a similar procedure as in the RRDE experiments. A combination of light sources, a deuterium lamp (Mikropack D-2000) and a halogen lamp (Ocean Optics HL 2000 — FHSA), were used in the setup. These sources were combined using an optical fiber arrangement and this fiber acted as the illumination source for the transmission measurements. The setup also included a spectrometer (Ocean Optics, Maya 2000 Pro), which was used to capture the transmitted light. The setup was aligned in such a way that the platinum/FTO sample was illuminated from the back side and the transmitted light was captured on the opposite side of the electrochemical cell. The transmission data was continuously recorded in situ, while performing the electrochemical measurements. All spectra shown were referenced to the Pt surface conditioned at 0.4 V vs RHE, and are an average of five measurements.

Results and Discussion

Kinetics of the BER and CER.—We first discuss some fundamental kinetic aspects of Br^- and Cl^- oxidation based on existing literature. Both the BER and CER are multistep reactions involving the transfer of two electrons, and the literature typically assumes the involvement of a single adsorbed intermediate.[31–35] Taking the CER as example, the elementary reaction steps considered are termed Volmer, Tafel and Heyrovský, which correspond to electrochemical adsorption, recombination and electrochemical desorption, respectively[36]:

$$Cl^- + * \rightleftarrows Cl* + e^- \quad \textit{Electrochemical adsorption (Volmer step)} \quad [1]$$

$$2\,Cl* \rightleftarrows Cl_2 + 2* \quad \textit{Recombination (Tafel step)} \quad [2]$$

$$Cl^*{+}Cl^- \rightleftarrows Cl_2 + e^- + * \quad \textit{Electrochemical desorption (Heyrovsk step)} \quad [3]$$

where Cl* is the adsorbed chlorine intermediate. An alternative mechanism has been proposed by Krishtalik.[34] This mechanism is generally only expected to occur on metal oxides,[31] but will be included for completeness. It assumes a second type of chlorine intermediate:

$$Cl^* \rightleftarrows Cl^{*+} + e^- \quad [4]$$

$$Cl^{*+} + Cl^- \rightleftarrows Cl_2 + * \quad \textit{Desorption (Krishtalik sequence)} \quad [5]$$

In this reaction sequence, Eq. 4 is assumed to be rate-limiting.

In the simplest method of deriving theoretical current-potential relationships from the above reactions, the Volmer step is taken as being in quasi-equilibrium, with the subsequent rate-limiting step as either recombination (Tafel) or electrochemical desorption (Heyrovský or Krishtalik). The observed current density then becomes dependent on θ_{Cl}, the surface coverage of chemisorbed chloride Cl* as a fraction of the maximum (saturation) coverage. In the mean-field Langmuir approximation, it is given by:[36]

$$\theta_{Cl} = \frac{K_{Cl}[Cl^-]e^{fE}}{K_{Cl}[Cl^-]e^{fE} + 1} \quad [6]$$

In Eq. 6, E is the applied potential, K_{Cl} is the chloride adsorption constant at $E = 0$, $[Cl^-]$ is the chloride concentration, and $f = F/(RT)$. In case of a Volmer-Tafel (V-T) mechanism, the current-potential relation is then given by

$$j_{VT} = 2Fk_T(\theta_{Cl})^2 = 2Fk_T\left(\frac{K_{Cl}[Cl^-]e^{fE}}{K_{Cl}[Cl^-]e^{fE} + 1}\right)^2 \quad [7]$$

Here, k_T is the (non-electrochemical) rate constant for Cl* recombination. Only the irreversible potential region is considered, such that the backward reaction may be neglected. For the Volmer-Heyrovský (V-H) mechanism, the resulting $j - E'$ relationship is

$$j_{VH} = Fk_H e^{\alpha_H fE}[Cl^-]\theta_{Cl} = Fk_H\frac{K_{Cl}[Cl^-]^2 e^{(\alpha_H+1)fE}}{K_{Cl}[Cl^-]e^{fE} + 1} \quad [8]$$

where k_H is the rate constant of the Heyrovský reaction for $E = 0$, and α_H is the corresponding transfer coefficient. Again, only the forward Heyrovský reaction is considered.

Derivation of limiting cases of Tafel slopes and reaction orders from the above mechanisms are demonstrated in the SI. In the V-T mechanism, the Tafel slope $b = \frac{\partial E}{\partial \log(j)}$ is expected to vary between 30 mV dec^{-1} $\leqslant b < \infty$, and the reaction order in Cl^- is $\mathcal{R}_{Cl^-} = 2(1 - \theta_{Cl})$, meaning it can vary according to $0 \leqslant \mathcal{R}_{Cl^-} \leqslant 2$. Both the V-H and the Volmer-Krishtalik (V-K) mechanism predict that 40 mV dec^{-1} $\leqslant b <$ 120 mV dec^{-1}, under the standard assumption that $\alpha \approx 0.5$. They differ in their expected reaction order: in the V-H case, $\mathcal{R}_{Cl^-} = 2 - \theta_{Cl}$, such that $1 \leqslant \mathcal{R}_{Cl^-} \leqslant 2$; the reaction orders in the V-K case are $\mathcal{R}_{Cl^-} = 1 - \theta_{Cl}$, such that $0 \leqslant \mathcal{R}_{Cl^-} \leqslant 1$. We note that Tafel analysis can prove very useful for kinetic investigations, but the "meaning" of the slope can be obfuscated by a wide variety of phenomena.[33,37,38] There is also significant width and overlap of the predicted Tafel slopes between the various mechanisms. One must thus exert caution when using Tafel values as a comprehensive diagnosis of the "real mechanism."

The experimental CER kinetics on Pt appear the most compatible with the V-T mechanism, as suggested by Conway and co-workers. Evidence comes from impedance studies,[32] potential-relaxation experiments[39] and recombination test plots,[40] showing that Eq. 7 gives a good fit of the experimental data. However, the interpretation of experimental reaction orders has been much less straightforward. This has been suggested to be in large part due to the complicating effect of transient formation of platinum oxide (PtO_x), which readily occurs at potentials where the CER takes place (see section 'Chloride oxidation and the effect of bromide'). The oxide layer competes with Cl^- adsorption during CER electrocatalysis, and may itself have an effect on intrinsic catalytic rates.[41,42] Conway and Novák obtained chloride reaction order values close to 1 when $[Cl^-] = 100$ mM, decreasing to zero when $[Cl^-]$ increased to 1 M and higher.[21] These values were measured at constant overpotential, for which the V-T mechanism predicts that $\mathcal{R}_{Cl^-} = 0$ (see section 'Reaction orders measured versus constant overpotential' of the SI). The authors explained the non-zero values by the effect of specifically adsorbed chloride anion (Cl^{-*}) on the PtO_x layer, but no further analysis was undertaken to explore this.

The BER mechanism on Pt has been much less studied,[43–45] but previous work by Conway et al. with similar methodology as used for the CER indicates that it follows the V-T characteristics when $[Br^-] > 1$ M.[22] The bromide reaction order was however not investigated in their work. The effect of oxides during the BER is expectedly much lower, because the BER takes place at lower potentials than the CER. Additionally, bromide has a much stronger oxide suppressing effect compared to chloride.

In a mixed $Br^- + Cl^-$ electrolyte, the situation becomes more complex, since multiple electroactive species are involved with differing adsorption strengths.[46] We will focus our study on mutual competitive blocking effects, since these should be relevant to the catalytic activity in an actual electrolyser. Additionally, co-adsorption of the two halogens could lead to the evolution of interhalogen compounds, such as BrCl; we will show below that this compound may indeed be electrochemically formed. We consider the direct electrochemical formation of triatomic interhalogen ions through a trimolecular reaction, such as $BrCl_2^-$, to be highly improbable.

Considerations of interhalogen formation reactions.—When carrying out electrolysis in a mixture of halogen anions, we need to consider various electrode reactions and solution reactions, as summarized in Scheme 1. The corresponding equilibrium constants of these reactions are given in Table S I.[29,47]

In Scheme 1, the solution phase interconversions are drawn in order of increasing thermodynamic stability, starting from Cl_2 and progressing toward Br_3^- as the most stable species. The overall pathway is divided in two segments: region 1 comprises the interconversion between stronger oxidizing species Cl_2, $BrCl_2^-$ and BrCl, whereas region 2 consists of Br_2, Br_2Cl^-, and Br_3^-, weaker oxidizing species with higher stability. Besides effects of kinetic competition, we are interested if electrocatalytic interhalogen formation can occur in a mixture of Br^- and Cl^-. As discussed previously, the main reaction of interest is the formation of BrCl according to

$$Br^- + Cl^- \rightleftharpoons BrCl + 2\,e^- \quad [9]$$

This previously unreported reaction falls thermodynamically in-between the BER and the CER. It is illustrated in the lower part of Scheme 1, along with the BER and CER, displaying the Tafel reaction (left) or electrochemical desorption (right) as the rate-limiting step. Unfortunately, accurate determination of products formed electrochemically on the electrode is not straightforward in this system, because the aqueous interhalogen reactions shown in Table S I and Scheme 1 are extremely rapid (values of rate constants are typically in the order of 10^9). Any "oxidizing equivalents" generated on the electrode will therefore tend to dissipate by reacting

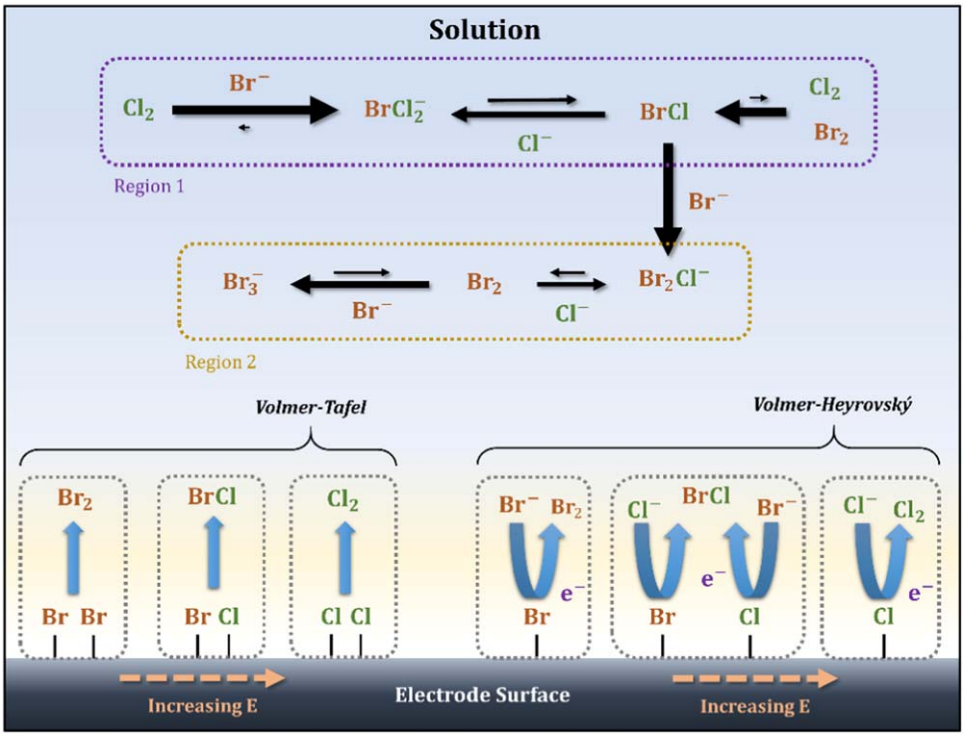

Scheme 1. Halogen reaction pathways on Pt during the parallel oxidation of aqueous Br^- and Cl^- in an acidic solution, according to data from literature[47] and Table S I. Black arrows represent solution phase reactions, relative sizes and thicknesses between pairs are illustrative of the direction of the corresponding equilibrium. Blue arrows represent elementary steps in electrochemical reactions on the electrode surface. Bottom area left shows rate-limiting reaction steps according to the Volmer-Tafel mechanism, which most likely dominates on Pt; the right shows rate-limiting reaction steps according to a Volmer-Heyrovský or Volmer-Krishtalik-type mechanism. We exclude trimolecular reactions in this scheme.

with bulk surplus of Br^- and Cl^- in solution, which obfuscates the identity of the electrochemical product originally formed.[48] Given sufficient mixing, the system will always evolve towards a mixture of Br^-, Cl^-, Br_3^-, Br_2Cl^- and Br_2, regardless of the electrode potential applied. Considering this, there are limitations to resolving electrochemical oxidation reactions involving interhalogen formation, but there are still factors that "strain" the system and allow a degree of deconvolution. Most importantly, one can observe in Scheme 1 that the reaction of BrCl with Br^- to form Br_2Cl^- is highly favourable (Table S I). Conversely, the concentration of BrCl in a mixture of Br^-, Br_2 and Cl^- is extremely low, and measurable quantities of BrCl can only result from an electrochemical driving force, which is then significantly larger than that required for Br_2 formation. It must be noted that when the potential is high enough to allow Cl_2 evolution, all species in Scheme 1 can in principle be formed chemically; chlorine may react with Br_2 to form BrCl by via the reverse of the dissociation reaction shown in Table S I ($1/K_D = 200$), as well as with Br^- to form $BrCl_2^-$. The most interesting potential region regarding surface-bound reactions is thus "in-between the BER and CER."

RRDE studies of parallel oxidation of bromide and chloride.— We used RRDE voltammetry to study the kinetics of parallel oxidation of Br^- and Cl^- under hydrodynamic conditions, as this greatly simplifies the analysis by keeping the diffusion layer thickness constant for a given reactant species. It also removes products from the surface that may possibly react further and in this way influence the apparent electrochemical kinetics[45]; this could be either follow-up electrochemical reactions on the surface, such as the oxidation of Br_2 into BrO_3^-, or through interhalogen reactions in the solution. The RRDE also allows following the formation of soluble reaction products by utilizing a Pt ring as detector. The ring potential was fixed at 0.7 V vs RHE, to reduce halogen species formed on the disk without also reducing O_2. Although the onset for oxygen reduction is around 0.95 V vs RHE on Pt in $HClO_4$, the adsorption of Br^- significantly increases the overpotential, reducing ORR to negligible rates for potential values down to 0.7 V vs RHE.[49] It was found that Br_2 reduction becomes diffusion limited at an overpotential of approximately 150 mV (see Fig. S 2 for details). Using similar methods, we previously showed that Cl_2 reduction on Pt becomes diffusion limited at overpotentials near 250 mV.[30] Ring currents at 0.7 V vs RHE can thus be taken as quantitative, because all reduction reactions of (inter)halogen compounds should be diffusion limited there.

Throughout this paper we generally use the NHE as potential scale. We note that the pH-dependent formation of platinum oxide (PtO_x) can have a large effect on the apparent reaction kinetics.[39,41,50] A change in acid concentration can thus cause a shift in the potential of oxidation of the Pt surface on the NHE scale, and correspondingly the catalytic activity. The significant background acid concentration of 0.1 M $HClO_4$ served to dampen pH changes as the total acid concentration was changed. The highest observed pH change was around 0.3 pH unit, when going from 100 mM $HClO_4$ to 100 mM $HClO_4$ + 10 mM HBr + 100 mM HCl, which is equivalent to a potential difference of about 20 mV.

Effect of scan rate and HCl concentration.—Figure 1 shows the BER and CER (panels A and B) as well as parallel Br^- and Cl^- oxidation (panel C) on a Pt-Pt RRDE, for varying scan rates. In Fig. 1a, the BER starts at a potential of 1.05 V, corresponding to a negligible overpotential, and reaches a plateau current at approximately 1.25 V. In control experiments using 5 mM HBr (not shown), the measured values of the BER limiting current correspond within a few % to a previous report by Xu et al.[45] The value is approximately 90% of the theoretical value predicted by the Levich equation, suggesting that the limitation stems from mass transport and that it is not due to kinetic limitations which may occur at much higher bromide concentrations.[22] The effect of scan rate on the BER is

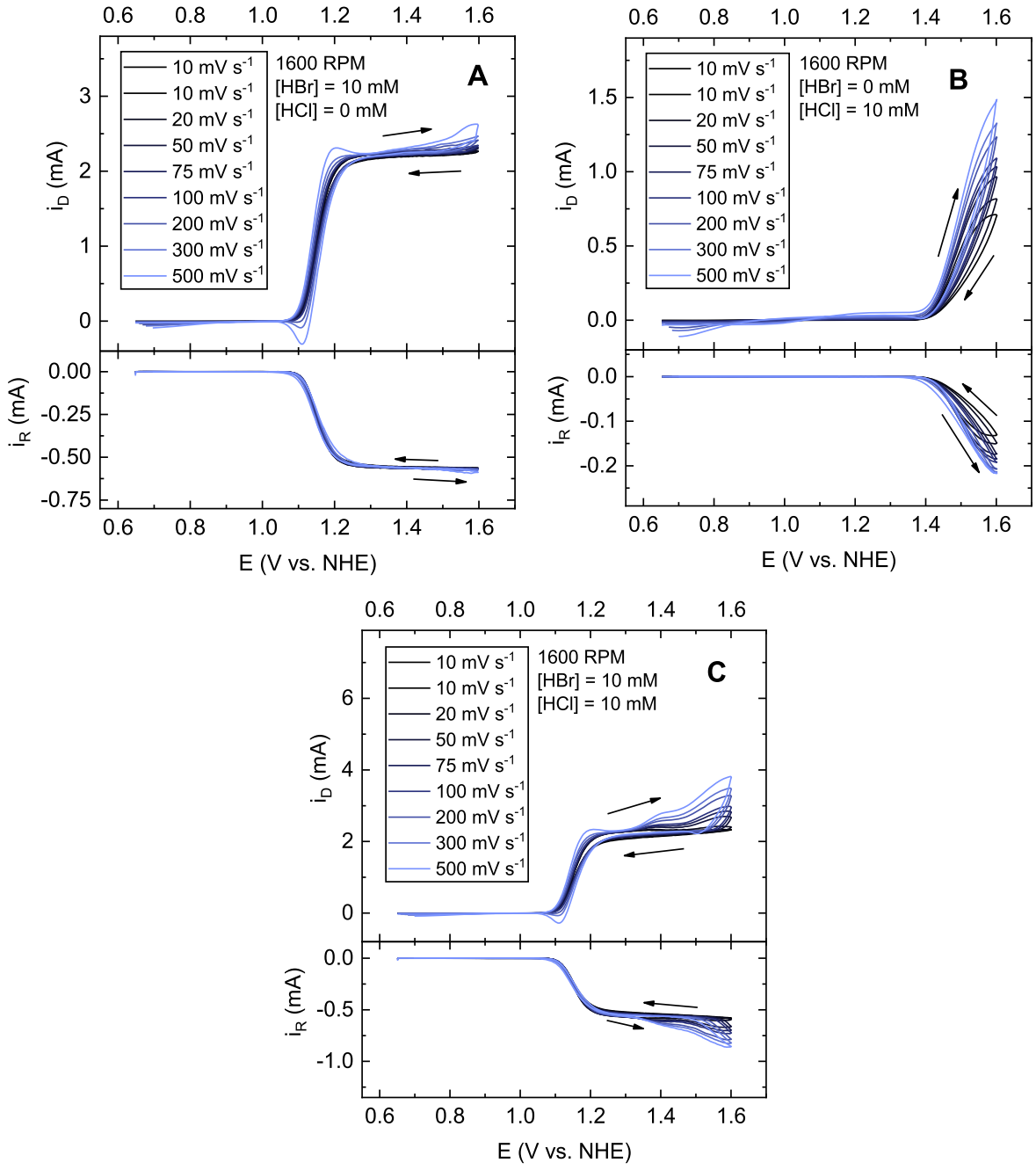

Figure 1. Cyclic voltammograms of a Pt-Pt RRDE in a solution of 0.1 M $HClO_4$, showing the BER in presence of 10 mM HBr (Panel A), the CER in presence of 10 mM HCl (Panel B), and parallel oxidation of Br^- and Cl^- in presence of 10 mM HBr + 10 mM HCl (Panel C). Varying scan rates are shown in shades of blue at a fixed rotation rate of 1600 RPM. Top panels show disk currents, bottom panels show ring currents while keeping the ring potential at 0.7 V. Arrows indicate scan direction.

minimal for slow to modest scan rates up to 75 mV s^{-1}. At higher scan speeds, the inability of Br_2 to be transported away from the surface fast enough leads to additional reactions; the oxidation of Br_2 to BrO_3^- is visible around 1.50 V in the forward scan,[51] as well as the reduction of Br_2 to Br^- in the backward scan near 1.10 V. The CER in Fig. 1b starts at 1.37 V, which like the BER is very close to its thermodynamic value. Contrary to the BER, it has a rather strong scan rate dependence. This effect can be explained by transient oxidation of the Pt surface. PtO_x has very poor catalytic activity for CER, and its formation is a relatively slow process on the timescale of this experiment.[22,32] A faster scan rate then leads to a Pt surface that is less oxidized when CER becomes thermodynamically favourable, and thereby results in higher reaction rates. This will be discussed in more detail below.

In Fig. 1c, the presence of both 10 mM HBr and 10 mM HCl leads to the same current plateau as seen in the BER wave in Fig. 1a, followed by two superimposed current waves, a first with an onset around 1.30 V, and a second one with an onset potential of 1.42 V. The latter one should correspond to CER; the wave starting at 1.30 V must correspond to the interaction between bromide and chloride. We will analyse the competition between BER and CER and their interaction in more detail in the subsequent sections.

Figure 2 shows parallel Br^- and Cl^- oxidation with varying HCl concentration, for two different scan rates. It is clear that the superimposed oxidation wave between 1.30–1.65 V is chloride concentration dependent, including the "pre-peak" that starts around 1.30 V. They experience an increase in current and lowering of the onset potential with increasing Cl^- concentration. The pre-peak is

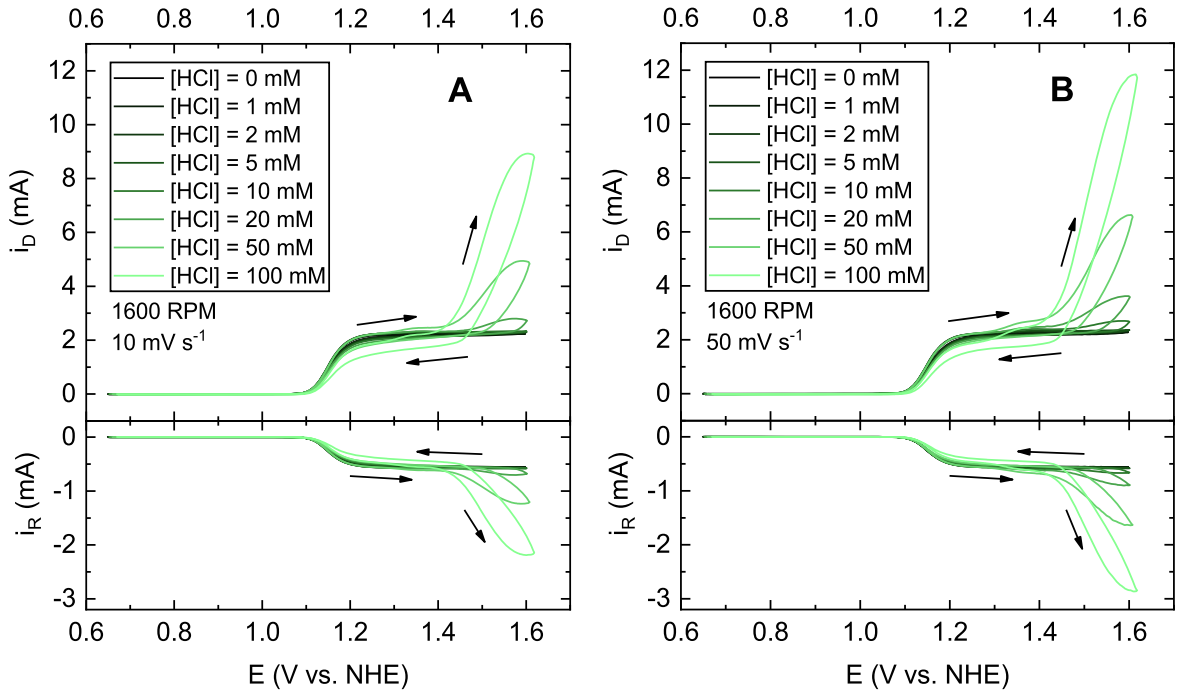

Figure 2. Cyclic voltammograms of a Pt-Pt RRDE in a solution of 0.1 M $HClO_4$ + 10 mM HBr, showing the effect of varying HCl concentrations in shades of green, recorded at 10 mV s^{-1} (a) and 50 mV s^{-1} (b) at a fixed rotation rate of 1600 RPM. Top and bottom panels like those described in Fig. 1. Arrows indicate scan direction.

also clearly captured in the ring currents (Fig. 2 bottom panels), so that it must correspond to a halogen evolution reaction. Diffusion-limited bromide oxidation (potential region of 1.20–1.30 V) seems rather unaffected by the increasing chloride concentration, except when $[Cl^-] = 100$ mM, where a kind of inhibition occurs.

The Pt ring electrode was used to quantify the extent to which the currents observed on the disk corresponded to the evolution of soluble product species (Figs. 1 and 2, bottom panels). The ring currents in Fig. 1 clearly mark the onset of the halogen oxidation reactions; in Fig. 1c particularly, the ring effectively mirrors the disk during halogen oxidation. Once halogen oxidation reactions start occurring, the ratio $|i_R/i_D|$ generally converges to a constant value that is within 2% of the RRDE collection factor (Fig. S 4 and Fig. S 5). Scan rates faster than 100 mV s^{-1} lead to some deviation from steady-state values, due to pseudocapacitive contributions on the disk (such as from PtO_x-related processes), as well as a decrease in the time resolution of the ring response.[52] At high CER overpotentials in high Cl^- concentrations we also saw systematic deviations (Fig. S 7 and Fig. S 8), likely because the ring response became distorted by bubble formation during intense gas evolution on the disk.[53] In low Cl^- concentrations, all scan rates show a slight decrease in ring/disk ratios above 1.55 V, likely due to the onset of slow parallel evolution of O_2 on the disk. The OER contribution on the disk is nonetheless rather small (less than 1%). In summary, all disk current can be ascribed to only halogen oxidation for any combination of [HCl], scan rate or rotation rate, as long as the scan rate does not exceed extreme values (see also Fig. S 6).

It has been reported previously that chloride significantly enhances the electrochemical dissolution of Pt, via complexation with the metal.[54,55] Although this represents a durability issue for practical Pt electrocatalysts, we do not expect this to affect our RRDE studies. The extent of dissolution per cycle is relatively small (approximately a few % of a monolayer), and takes place mainly in the negative-going scan, during the reductive dissolution of the oxide layer. In this study we use data from the forward scans almost

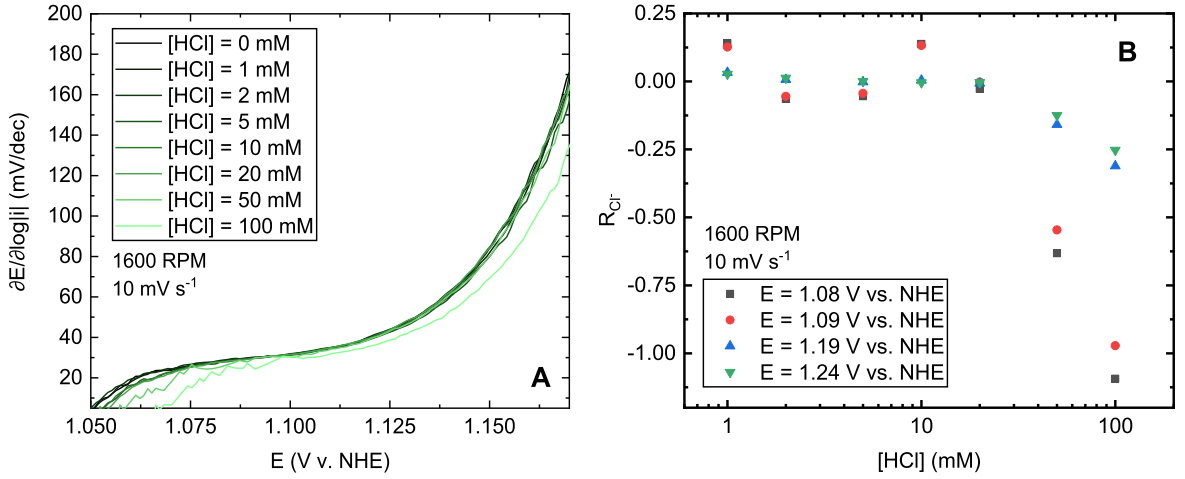

Figure 3. Tafel slope values in the bromide oxidation region of Fig. 2a for various measured chloride concentrations. Only forward scans are shown. B: Chloride reaction order $\mathcal{R}_{Cl^-}$ as function of chloride concentration, based on data shown in Fig. S 11B.

exclusively. As the electrodes used in our study are polycrystalline, we would also not expect the surface area to change significantly under dissolution. The effect of dissolution on the results presented here are thus expectedly negligible, as previously suggested by Novák and Conway.[56]

Bromide oxidation and the effect of chloride.—In this section, we look more closely into the effect of chloride on the oxidation of bromide, primarily by investigating Tafel slopes, reaction orders and the effect of mass transport. Koutecký-Levich plots of the bromide oxidation wave at various chloride concentrations were constructed using the forward sweeps of CVs (See Fig. S 12). The y-intercepts were then calculated as function of potential (Fig. S 13). These results show that a higher [Cl^-] causes an increasing degree of kinetic control over the reaction, although the effect is very subtle when [Cl^-] $<$ 100 mM.

Figure 3a shows Tafel slopes (derived from Fig. S 10B) as a function of potential. From Fig. S 13, we can discern the potential region of roughly 1.075–1.125 V as kinetically limited; in this region the Tafel slopes show a fairly constant value between 25–35 mV/dec, agreeing well with previously reported values.[22] Addition of chloride up to concentrations of 50 mM does not change the Tafel slope values, and chloride reaction order analysis (Fig. 3b) shows that $\mathcal{R}_{Cl^-}$ stays close to 0. The effect of changes in PtO_x coverage due to varying pH should be very minor; control experiments with 10 mM HBr and no chloride showed that the BER rates show no hysteresis up to 1.40 V, suggesting that inhibiting PtO_x, though it may be formed,[44] plays no significant role in the apparent catalytic activity (Fig. S 14). The reaction becomes notably affected when the chloride concentration increases further to 100 mM, where the Tafel slope values rise less quickly as function of potential, and $\mathcal{R}_{Cl^-}$ decreases to around -1.

We also measured the BER dependence on bromide, in absence and presence of an excess of chloride as to further probe the latter's competition behaviour. Figures S 15 and S 16 show bromide oxidation curves and derived Tafel slopes as function of [Br^-]. Tafel slope values of the BER in 1 M HCl (Fig. S 16B) are overall higher (30–50 mV dec^{-1}) and significantly less linear, as would be expected on the basis of Langmuirian competitive adsorption (Section 'Thermodynamic data of (inter)halogen species' of the SI). Figure S 17 displays $\mathcal{R}_{Br^-}$ for 10 mM $\leqslant$ [Br^-] $\leqslant$ 100 mM; the values around each given [Br^-] are shown vs potential, because the BER is too fast to measure activation controlled currents over a wider range of [Br^-] at a fixed potential, without running into diffusion limitations. The quasi-linear regions in Fig. S 16 were used to approximate the activation-controlled region for each [Br^-]. Experimental error from very small currents and the possible influence of the backward reaction led to unexpectedly high values of $\mathcal{R}_{Br^-}$ at very low overpotentials; nonetheless, for each [Br^-] in their respective activation controlled potential region, $\mathcal{R}_{Br^-}$ values are arguably close to 2, as predicted by the V-T mechanism. The apparent reaction orders rapidly approach 1 as the potential increases, due to mass transport control. Interestingly, Ferro et al. obtained $\mathcal{R}_{Br^-} \approx 1$ on a stationary Pt electrode[51]; these values were obtained at constant overpotential, by keeping the value of E_{eq} fixed by adding equimolar amounts of Br^- + Br_2. In this case, the expected values of $\mathcal{R}_{Br^-}$ are within 2 and 0. Considering the rather narrow (roughly 50 mV) potential ranges in Fig. S 17 where the BER appears activation controlled, it is possible that their values were unintentionally obtained under diffusion controlled conditions.

When regarding the effect of competitive Cl^- adsorption, one can extend the bromide adsorption isotherm to include both Br^- and Cl^- according to

$$\theta_{Br} = \frac{K_{Br}[\mathrm{Br}^-]e^{f\!E}}{K_{Br}[\mathrm{Br}^-]e^{f\!E} + K_{Cl}[\mathrm{Cl}^-]e^{f\!E} + 1} \qquad [10]$$

A detailed discussion of the mechanistic implications of Eq. 10 can be found in the SI. Importantly, Eq. 10 leads to the same predictions for $\mathcal{R}_{Br^-}$ as in absence of competition; namely, that $\mathcal{R}_{Br^-}$ should consistently decrease from 2 to 0 as a function of [Br^-] in the V-T mechanism. In presence of an excess of 1 M Cl^- in Fig. S 17A, $\mathcal{R}_{Br^-}$ has overall slightly lower values; the reaction is no longer fully diffusion-controlled such that $\mathcal{R}_{Br^-}$ is no longer strictly 1 at higher potentials. The data seem to approach a non-zero value with higher potential, and again approach 2 at low overpotentials. Both observations are predicted by the V-T pathway under the assumption of Langmuirian, competitive adsorption. From this, we conclude that chloride acts as an inhibitor on bromide oxidation and is otherwise uninvolved. Because chloride typically binds weaker to surfaces than bromide,[57] we expect that only at high ratios of chloride vs bromide (such as in seawater), where $K_{Br}[\mathrm{Br}^-] \ll K_{Cl}[\mathrm{Cl}^-]$, the BER may become significantly slowed down.[58]

Chloride oxidation and the effect of bromide.—In this section, we look more closely how the oxidation of chloride is affected in a mixed Br^- + Cl^- electrolyte. The pre-peak starting at 1.30 V (Figs. 1 and 2) suggests a more complex Br and Cl interdependence than only competitive adsorption, which is most likely due to the formation of BrCl; we will discuss the nature of this process separately (vide infra).

For a meaningful analysis, it is necessary to isolate the chloride oxidation current from the superimposed BER current. A strict separation is complicated, because the oxidation pathways of Br^- and Cl^- are clearly mutually dependent, and the underlying contribution of each is not exactly known. However, results in the section 'Bromide oxidation and the effect of chloride' and Fig. S 13 indicate that the BER generally becomes diffusion limited at potentials much lower than chloride oxidation. Between 1–50 mM chloride, we observed no signs that bromide oxidation was still kinetically controlled at potentials higher than 1.20 V vs NHE (Fig. S 13); the measurement at 100 mM chloride appears to be a borderline case. From the chemical nature of the Tafel recombination step, this implies that the reaction rate can still increase to sufficient values for the reaction to reach diffusion limitations, despite competitive chloride adsorption. Bromide oxidation is thus expected to follow a sigmoidal curve, which can be modelled and subtracted to yield only currents from chloride-related processes. We fitted the BER wave using a 5-parameter generalised logistic function, whose relative complexity allowed modeling the asymmetry that is inherent to reaction mechanisms more complex than a single electron transfer step.[59] The fitting procedure is illustrated in Fig. S 26.

Figure 4 shows the effect of various experimental parameters on the current related to chloride oxidation, after applying a logistic baseline correction for the superimposed BER current. In comparison with the dashed traces of "pure CER current" under bromide-free conditions, there are significant differences. The "main" oxidation wave, with an onset of 1.45 V in Fig. 4a, can be ascribed to the CER. The overpotential for CER in Figs. 4a and 4b is generally increased relative to bromide-free conditions, except for the experiments with the highest scan rates and chloride concentrations. Figure 4c furthermore shows that the CER current slightly decreases with rotation rate. This behavior may be caused by an increase of the steady-state bromide coverage θ_{Br} as a result of increased mass transport, leading to suppression of the CER; when [Cl^-] was increased to 100 mM such that the BER became more inhibited, the CER displayed an increase in current with rotation rate, but a more clear rotation rate dependence could not be established (Fig. S 18).

The CER is much more likely to be affected by PtO_x formation, for which the driving force is significant near the CER equilibrium potential. Oxide growth causes the CER current in Fig. 4 to level off or sometimes even decrease with higher potential. The highest recorded currents in Fig. 4b are less than 10% of the diffusion limitation predicted by the Levich equation, showing that the reactivity limitation is a kinetic effect.

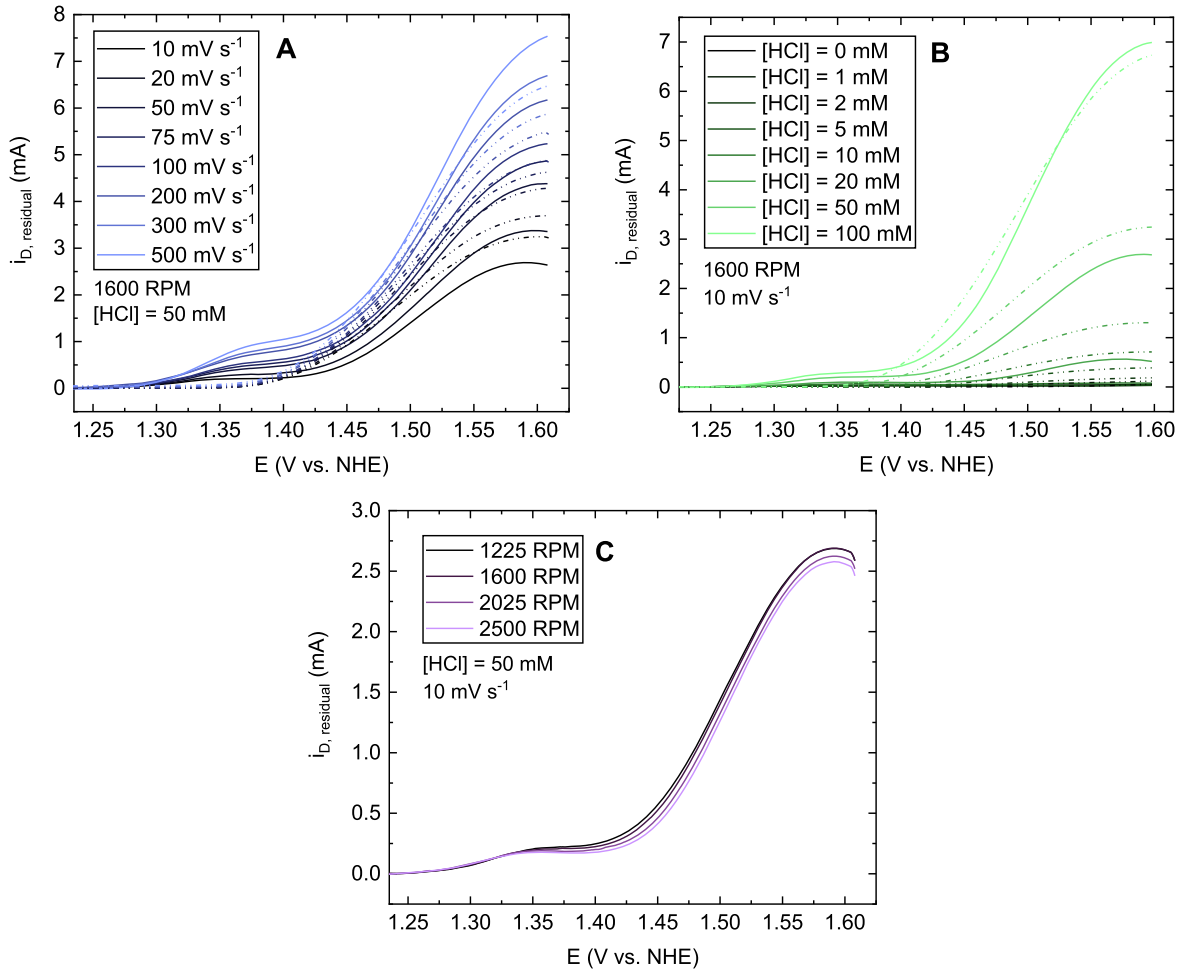

Figure 4. Residual chloride oxidation currents after subtraction of BER-related current (10 mM HBr) using a generalised logistic baseline. Shown are the effect of scan rate (a), HCl concentration (b), and rotation rate (c). Dashed lines in a and b correspond to CER data measured in absence of Br^- under otherwise identical conditions.

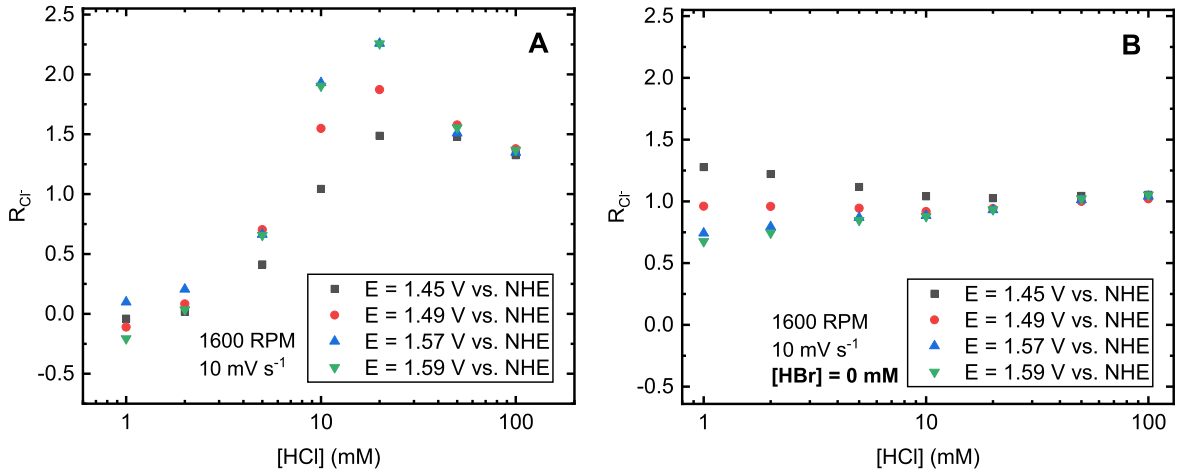

Figure 5. Chloride reaction order $\mathcal{R}_{Cl^-}$ as function of chloride concentration, based on data from Fig. 4b. Shown are values in presence of 10 mM HBr (a), as well as those in bromide-free conditions (b).

Figure 5 shows chloride reaction orders based on data from Fig. 4b. In presence of Br^- (Fig. 5a) the reaction order is close to 0 at low chloride concentration, but then increases to values close to 2, and then assumes a value of $\sim$1.4 at $[Cl^-] = 100$ mM. This is in remarkable contrast to the results obtained in absence of Br^- (Fig. 5b), for which reaction orders are close to 1, regardless of potential or chloride concentration.

All results in Fig. 5 should contain a contribution from transient formation of the PtO_x layer. For the CER, this "oxide reaction order" has been studied previously by Conway and Novák, who obtained steady $\mathcal{R}_{Cl^-}$ values between 0.8−0.9 which quite suddenly decreased to 0 as $[Cl^-]$ increased to 1 M (see also section 'Kinetics of the BER and CER'). These values were derived at constant overpotential, in which case the V-T mechanism predicts that $\mathcal{R}_{Cl^-}$ is always zero; the

contradicting non-zero values were ascribed to specific adsorption by Cl^- at the expense of the oxide layer, forming co-adsorbed "Cl^-*" which saturates to a constant value at higher concentrations. This explanation is however not completely sufficient, since the surface reaction order $\frac{\partial \ln \theta_{Cl}}{\partial \ln [Cl^-]}$ is then expected to vary between 1 and 0, and thus the overall reaction order should again be $0 \leqslant \mathcal{R}_{Cl^-} \leqslant 2$; most importantly, $\mathcal{R}_{Cl^-}$ should not be consistently near unity, but should vary as a function of $[Cl^-]$ and potential. The V-T mechanism predicts the same when measurements are made at constant potential, such as in our results in Fig. 5b; like Conway and Novák's results, they do not agree satisfactorily with the usual kinetic models.

Br^- is also known to inhibit the oxidation of platinum, and does so more strongly than Cl^-.[43,56] Br^- may thus affect the CER indirectly by replacing PtO_x as the competitive adsorbate, which could change the apparent reaction order values between Figs. 5a and 5b. To look into this more closely, one could describe the effect of adsorption from either Br^- or PtO_x using a site-blocking model. From previous studies, it is known that the oxide layer on Pt initially forms up to a monolayer of OH*, and O*, coupled to a slow place-exchange between O and Pt as oxidation progresses.[60,61] For a fixed potential E, this oxide growth depends on time according to[41]

$$Q_{PtO_x}(t) = A(E)\log(t + t_0) \approx A(E)\log(t) \qquad [11]$$

In this equation, Q_{PtO_x} is the charge transferred in the formation of the layer, which can be measured from the corresponding reduction peak, t_0 is a offset time present at the start of the linear $\log(t)$ region (usually, $t_0 \ll t$), and A is an empirical constant that depends on the potential. The oxide growth has been reported to depend on time as $\log(t)$ over a wide range of time and potential values, including when chloride is present in the electrolyte.[41] In our potentiodynamic experiments, the overall polarization time and thus the expected oxide thickness should then approximately depend on the scan rate ν for a given potential window and electrolyte composition according to

$$Q_{PtO_x} \propto \log\left(\frac{1}{\nu}\right) \qquad [12]$$

Values of Q_{PtO_x} were obtained from the PtO_x reduction peak (Fig. S 19). As predicted by Eq. 12, a plot of Q_{PtO_x} vs $\log(\nu)$ resulted in a straight line with negative slope in 0.1 M $HClO_4$. This relationship was preserved in presence of 10 mM Br^- (Fig. S 20). It was also preserved in combined presence of Br^- + Cl^- (Fig. S 21), suggesting that PtO_x shows the same growth characteristics under influence of the two halogen anions. When then comparing CER current values vs Q_{PtO_x}, a quite linear relationship emerges (Figs. S 22 and S 23). We can reasonably assume that sub-monolayers of oxide were present during most experiments, since in our case the charge of a "monolayer" oxide on a perfectly flat surface corresponds to roughly 80 μC[41]; the results thus suggest that the effect of PtO_x on the CER activity is primarily through site-blocking. A similar observation underlies the work of Patil et al.[62] Further evidence comes from Fig. S 24, where CER currents recorded at 1.57 V (high overpotential) were extrapolated to $Q_{PtO_x} = 0$. These values, belonging to an "oxide-free" surface, corresponded quite well to predictions from the Levich equation (shown in blue), suggesting that the CER would reach diffusion-limited currents in absence of oxides at 1.57 V. There may additionally be an intrinsic catalytic effect of the oxide layer, but this is likely most significant at specific oxide coverages that are close to (formally) a monolayer.[21,41]

Contrary to PtO_x, the adsorption of Br^- is in pseudo-equilibrium and should be regarded in the same way as the CER, such as by using the competitive Langmuir isotherm in Eq. 10. However, the results from Fig. 5a strongly disagree with the prediction that $\mathcal{R}_{Cl^-}$ should consistently decrease from 2 to 0 as a function of $[Cl^-]$. Instead, $\mathcal{R}_{Cl^-}$ stays close to 0 for an appreciable concentration range and then increases. A simple Langmuirian site-blocking description therefore seems inadequate. The chloride reaction orders in Fig. 5a also seem incompatible with a change in reaction pathway towards BrCl formation, since it is expected that $\mathcal{R}_{Cl^-} \leqslant 1$ for this reaction.

Figure 6 shows measured Tafel slope values for the CER in presence (A) and absence (B) of Br^-. "Pure CER" in Fig. 6b for various chloride concentrations has linear Tafel regions with a slope between 35–45 mV dec^{-1}, in agreement with previous results,[50] followed by a continuous increase in slope with higher potential. The latter is explained by (transient) inhibition of the CER due to PtO_x formation, as was previously noted; it can be seen that the effect lessens as the chloride concentration increases. Like in Fig. 5, the presence of Br^- imparts significant changes. Intriguingly, the linear Tafel regions now have a value of around 100 mV dec^{-1}. In the Langmuir isotherm, competition leads to higher Tafel slope values (see Table S II), but only in combination with increasing curvature; it cannot explain Tafel regions that have a higher value, but also stay linear. The linear value of 100 mV dec^{-1} could imply that a change in the rate-determining step of the CER mechanism has taken place, the most straightforward possibility being rate-limiting Volmer discharge (Eq. 1). This, however, is in contradiction with $\mathcal{R}_{Cl^-}$ being greater than 1 in Fig. 5a. In summary, chlorine evolution seems to be the major reaction in the chloride oxidation region, but presence of Br^- induces a large change in the apparent kinetics. This change does not stem from a change in how the oxide layer forms

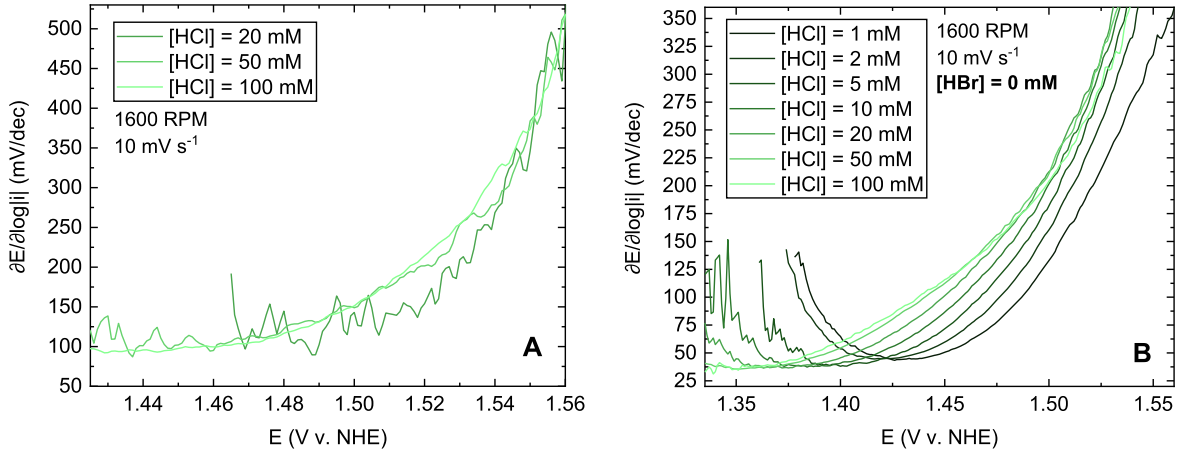

Figure 6. Tafel slope values in the CER region of Fig. 4b following the pre-peak, for the various measured chloride concentrations. Only forward scans are shown. Shown are values in presence of Br^- (a), and values for "pure CER" in absence of Br^- (b). Several traces in A and B involving 0–10 mM chloride have low signal/noise ratios and are not shown or have been cut off at lower potentials.

during the experiments, but seems to be the result of a complex interaction of Br^- or Br* with the CER reaction pathway on the surface. The CER on Pt, regardless of the presence of Br^-, is not captured by the usual microkinetic models in a fully satisfactory way, as was previously hinted at by Tilak and Conway.[36]

Nature of the chloride oxidation pre-peak.—As mentioned above, the pre-peak that starts at 1.30 V only appears when both Br^- and Cl^- are both present, at a potential where the BER is diffusion limited, and where the CER is thermodynamically not yet allowed, meaning it cannot be ascribed to the evolution of either Br_2 or Cl_2. At the same time, the pre-peak current is always registered on the ring, so that it is associated with the evolution of a soluble reaction product. Therefore, it likely involves formation of an interhalogen compound, where BrCl is the most probable candidate, as its standard potential (1.19 V vs NHE) lies in-between CER and BER.

To investigate the pre-peak in more detail, it was necessary to extend the fitting procedure discussed previously to "isolate" the relevant current. We note that the pre-peak is always convoluted by parallel BER and CER. The BER contribution was previously modeled using a generalised logistic function, such that the residual current contains the CER wave with the pre-peak superimposed. To isolate the pre-peak current, the CER wave was modeled using a simple exponential function according to the Butler-Volmer relation. CER curves were fitted using narrow potential regions where the Tafel slope was roughly constant as in Fig. 6. The resulting exponentials were then extrapolated under the pre-peak, forming a non-linear baseline together with the generalised logistic function for the BER. The multistep nature of the reaction could justify a more complex fitting function, but this relation need not hold at potentials higher than the linear Tafel regions, where the real kinetics are obscured by PtO_x formation. The entire procedure thus assumes that the BER and CER are the main reactions occurring in a mixed Br^- and Cl^- electrolyte, behaving respectively as an asymmetric sigmoid and (at low overpotentials) a superimposed exponential, and that the pre-peak is a third process overlapping with the previous two. In case that the CER currents were too small to observe a linear Tafel region, a simple linear baseline was used instead.

Figure 7 shows the pre-peak current determined after applying the two-step baseline to correct for the superimposed BER and CER currents, and its response to various experimental parameters. No effect from rotation rate is apparent, suggesting that the rate-limiting step is surface-confined; the peak also shows complex dependencies on scan rate and chloride concentration, as shown in Fig. 8.

In case of a surface-confined reaction, one would expect a linear dependence between peak current and scan rate, but this is not observed in Fig. 8. The pre-peak has a linear dependence of the peak current on the *square root* of the scan rate, an approximately linear dependence of peak charge with the inverse square root of the scan rate, and a "surface charge order" of about 0.5 (i.e. a square root relationship between peak charge and chloride concentration). Especially the linear dependency of peak current vs square root scan rate is striking. This outcome is usually expected for a solution species reacting at a stationary electrode, where the square root relationship arises from the dependence of the diffusion layer thickness on time; it should not apply under hydrodynamic conditions, where the thickness is constant in time. A possible explanation for this, as well as the general behavior of the pre-peak, is that surface diffusion is involved. Formation of BrCl is expected to proceed via an electrochemical Langmuir-Hinshelwood mechanism, such as during CO stripping from Pt,[63] which requires concerted steps of two different reaction surface species instead of one. We found that the pre-peak is effectively irreversible and does not re-appear in the backward scan, even when using a lower potential of scan reversal (Fig. S 27). This implies that it requires a precursor that is only formed during the forward scan (Fig. S 28).

UV–vis studies of parallel oxidation of bromide and chloride.—In the RRDE experiments, we ascribed the three main oxidation events to the formation of Br_2, BrCl and Cl^- on the basis of a kinetic analysis. It is highly desirable to corroborate these results with a method capable of ascertaining the identity of the products formed. UV–vis spectroscopy allows this, since all species in Table S I (except Br^- and Cl^-) have a secondary adsorption band (or shoulder, in case of Br_3^-) that falls in the range 325–390 nm, which is accessible when measuring a transparent electrode on a glass substrate. Stationary electrodes in quiescent solutions were used to minimize mixing of the electrolyte near the electrode surface, so that the lifetime of thermodynamically labile species was enhanced. We applied a stepwise potential vs time program constituting 25 mV steps with a 30 s duration, between 1.060–1.485 V vs NHE (Fig. S 29), to study both the effect of increasing potential, as well as shifts in solution composition during progressing oxidation reactions for each constant potential. Changes in the total transmission were measured after passing the beam through the back of the Pt/FTO electrodes and through the electrolyte, to probe the Pt interface as well as halogen species in the surface layer.

The spectra in Fig. 9 show the effect of increasing bromide concentration and were taken at potentials related to regions of interest, as seen in the corresponding currents in D. The BER has significant activity at 1.110 V (A) and reaches a plateau around 1.185 V (B). The CER becomes just possible at 1.335 V (C), based on the comparison with bromide-free experiments (red trace in D). Features seen in the spectra are always the sum of a mixture of species (see 'Considerations of interhalogen formation reactions'); in Fig. 9a, Br_3^- contributes the most strongly to the signal due to its high extinction coefficient.[47] Once the potential increases to 1.185 V (Fig. 9b), the dominant species is Br_2Cl^-. This can be explained by depletion of Br^- near the surface, which shifts the local equilibrium from Br_3^- to Br_2 and subsequent reaction with Cl^- (Scheme 1). This is supported by a strong correlation between the peak height relative to its shoulder at 383 nm and the extent to which the BER approaches the current plateau (Fig. S 31). Increasing the potential further to 1.335 V, where the CER is allowed to occur, leads to a substantial decrease in transmission in the region 320–360 nm. This is clearly related to the formation of Cl_2, $BrCl_2^-$ and BrCl in solution, which all adsorb in this wavelength window.

When examining the currents recorded in parallel with UV–vis in Fig. 9d, we once more observe a wave that precedes the CER onset (onset 1.260 V), and becomes more prevalent as the bromide concentration increases. This pre-wave corresponds quite well to results from the RRDE experiments, and suggests that BrCl is formed electrochemically. Further evidence from its formation comes from Fig. 10, where we regard the complete time evolution of a typical UV–vis experiment during parallel bromide and chloride oxidation. Between 1.110 V and 1.260 V, the spectra show the previously described peak of Br_2Cl^- near 380 nm. As the potential is stepped beyond 1.260 V, the transmission in the region 340–360 nm disproportionally lowers, which can only be caused by the formation of Cl_2, BrCl or $BrCl_2^-$. We note that in bromide-free conditions, Cl_2 becomes only just detectable around 1.350 V, and dominates at 1.400 V (Fig. S 32). The change at 1.260 V therefore implies the formation of BrCl or $BrCl_2^-$ without the presence of Cl_2 in solution, such that they must have been formed directly by BrCl formation on the electrode. We obtained similar results under conditions of higher bromide concentrations (Fig. S 33), as well as lower overall halide concentrations (Figs. S 34 and S 35). The UV–vis spectra thus confirm the observation in the RRDE experiments of an intermediate oxidation reaction occurring between the BER and CER.

In Fig. 9, we note an increase in transmission in the wide region of 550–900 nm for experiments involving high bromide concentrations combined with high potentials. This increase was likely caused by transient Pt dissolution during vigorous halogen oxidation. The used Pt samples had a low thickness of roughly 5 nm, to limit scattering of the beam; any dissolution thus had a relatively large effect on the transmission.

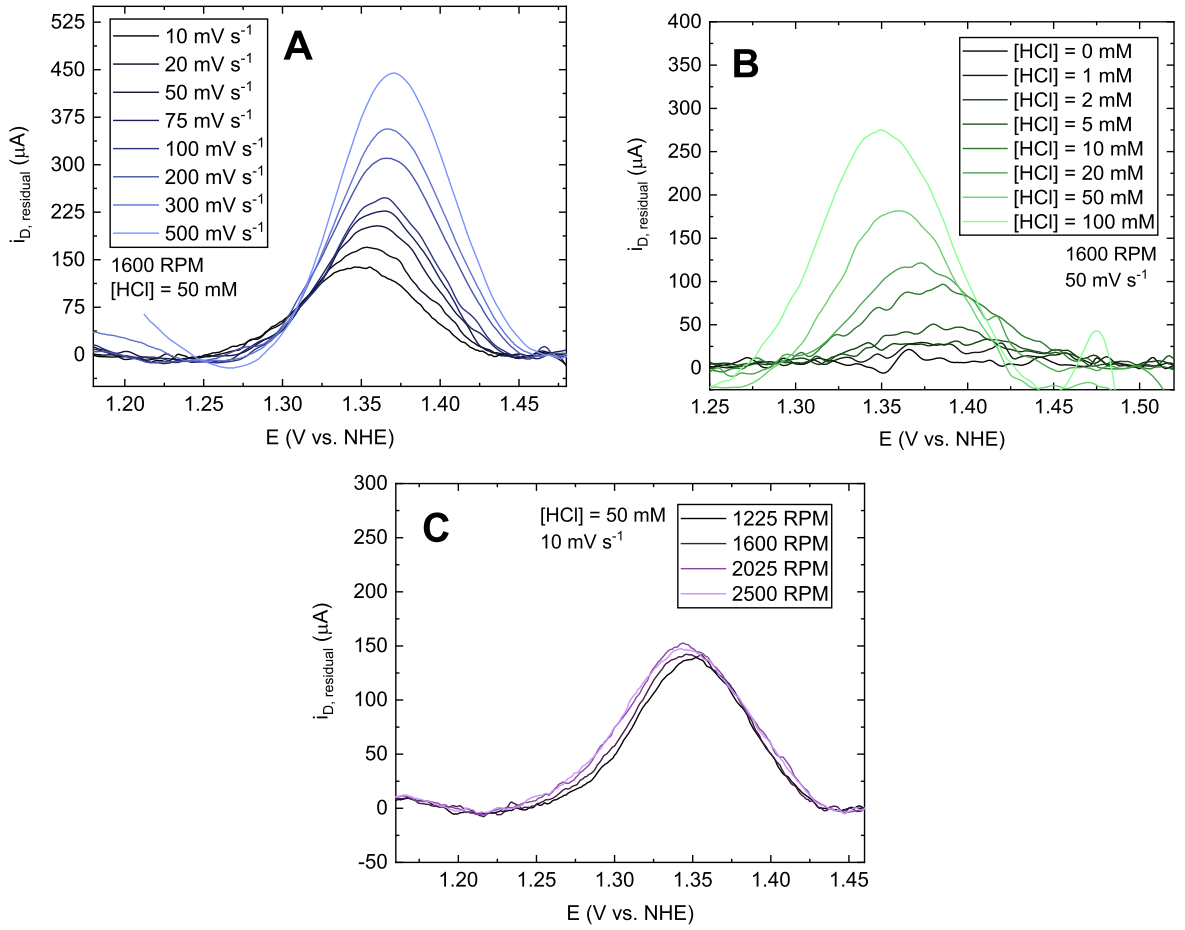

Figure 7. Examples of chloride oxidation pre-peak current determined from RRDE experiments, after separating BER and CER contributions using a generalised logistic and exponential function, respectively. Shown are the effect of scan rate (a), HCl concentration (b), and rotation rate (c).

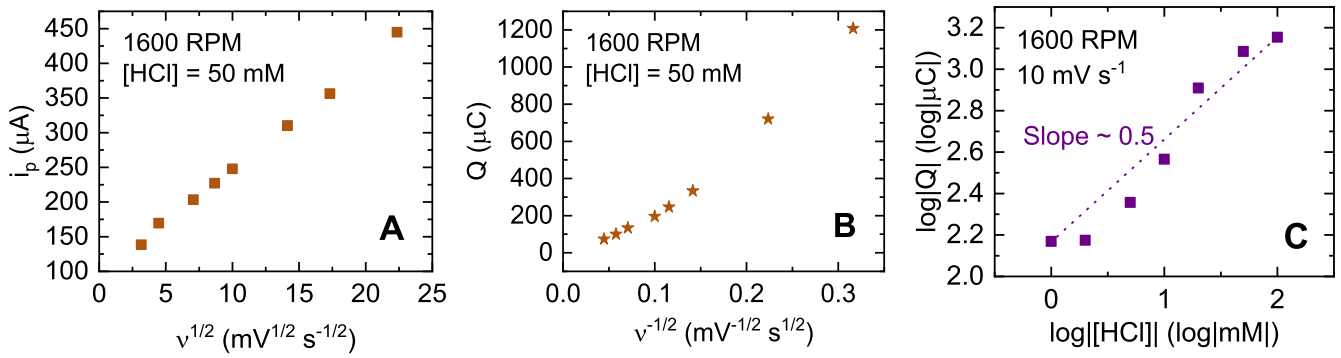

Figure 8. Scan rate and [Cl^-] relationships as determined for the CER pre-peak, using data from Fig. 7. Shown are the dependency of the peak current vs the square root of the scan rate (a), dependency of the peak charge on the inverse square root of the scan rate (b), and a log-log plot of the peak charge vs chloride concentration (c).

Discussion and Conclusions

The study of parallel Br^- and Cl^- oxidation on Pt revealed significant differences in their interaction. Bromine evolution exhibited linear Tafel slopes of 25–35 mV dec^{-1} and a Br^- reaction order $\mathcal{R}_{Br^-}$ that is probably close to 2 at low overpotentials. In the presence of chloride, the reaction becomes increasingly kinetically controlled, and Tafel curves have steeper slopes and becomes less linear. The BER chloride reaction order $\mathcal{R}_{Cl^-}$ progressed from roughly 0 to −1 as the chloride concentration [Cl^-] increases. All these phenomena could be quite well modeled by the Tafel recombination-controlled mechanism, describing the competitive adsorption of Br^- and Cl^- with a simple Langmuir isotherm in the Volmer pre-equilibrium. The results suggest that the effect of Cl^- on the BER is "simple" competitive adsorption through site blocking. The competing effect of Cl adsorption will likely become more prevalent at higher [Cl^-]/[Br^-] ratios, such as in seawater.

Contrary to the BER, the Langmuirian Volmer-Tafel approach fails for accurately modeling the CER kinetics and the competing effect of bromide, as neither the CER itself (in absence of Br^-) nor the CER during parallel Br^- and Cl^- oxidation are properly described by this model. In absence of Br^-, the CER displays linear Tafel regions between 35–45 mV dec^{-1}, and $\mathcal{R}_{Cl^-}$ values that are consistently close to 1, irrespective of [Cl^-] or potential *E*. The addition of Br^- again leads to linear Tafel regions but with

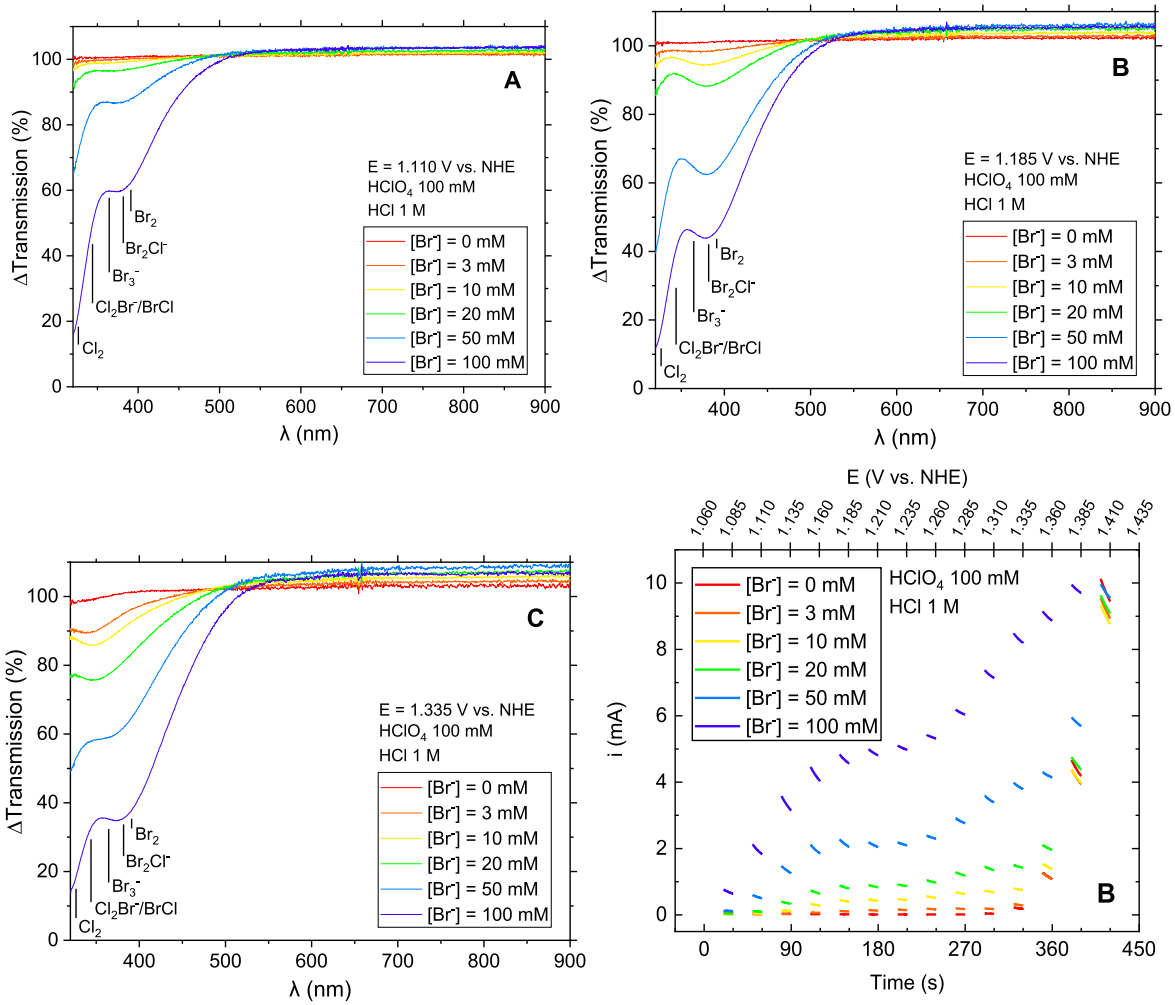

Figure 9. UV–vis measurements of a stationary Pt/FTO electrode in a solution of 0.1 M $HClO_4$ + 1 M HCl, in presence of various [HBr]. a, b and c: UV–vis spectra measured as function of bromide concentration, after stepping the potential up to 1.110 V (a), 1.185 V (b) and 1.335 V (c), in 25 mV steps of 30 s each. Spectra are shown of 10 s after applying the relevant potential. Previously published[47] wavelengths of peak adsorption are indicated for each relevant species. d: Corresponding currents measured during the experiments. Only the final 10 s of each potential step are shown for clarity (see Fig. S 30 for full data). Upper axis shows the potentials applied at each moment in time.

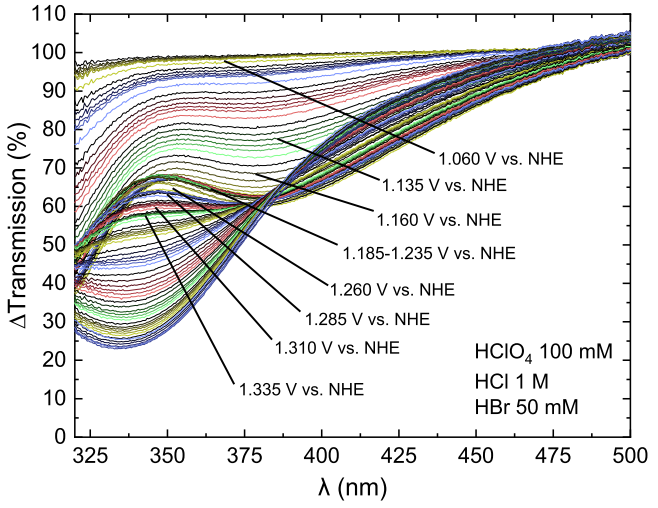

Figure 10. Complete set of UV–vis experiments for parallel bromide and chloride oxidation in 1 M HCl and 50 mM HBr, zoomed on the region where the halogen species adsorb. Colors denote different potential steps, some values of which are indicated; color gradients from dark to light indicate time evolution of the spectra during each potential step.

significantly higher values of ~100 mV dec^{-1}, and $\mathcal{R}_{Cl^-}$ varies between 0 and 2 as function of Cl^-. The parallel formation of a platinum oxide layer at CER-relevant potentials and its effect on the apparent oxidation kinetics remains an incompletely understood issue, but it should not be the origin of the Br^--induced drastic change in the CER kinetics. The supressing effect of 10 mM Br^- leads to a decrease of the PtO_x charges during CER experiments of 10%–30% (Figs. S 22 and S 23), but the oxide growth behavior was very similar to Br^--free conditions. It thus seems reasonable that the interaction of the PtO_x layer with the occurring CER, although not exactly understood due to its complexity, is not changed significantly by bromide. The change in CER kinetics should originate from a direct effect of Br^- on the adsorption and recombination of chloride.

In addition to the BER and CER, formation of the interhalogen BrCl likely takes place during parallel Br^- and Cl^- oxidation on Pt. Evidence for this comes from an oxidation "pre-peak" that thermodynamically precedes the CER, and UV–vis experiments that indicate that an "intermediate" oxidizing species is formed at potentials lower than the CER onset. RRDE experiments suggested that BrCl evolution takes place via an irreversible surface reaction with a dependence on scan rate, which suggests that surface diffusion plays a role; the process was strongly dependent on the preceding electrode treatment and probably depends on a specific intermediate.

This study has shown that 2-electron halogen oxidation reactions may still be more complicated than previously thought. While the BER conformed surprisingly well to a simple Langmuir pre-equilibrium model, previous studies on poly- and monocrystalline Pt surfaces show that the surface should be virtually saturated with Br* near the onset of the BER[64–66]; a similar argument holds for Cl* and the CER.[67–69] The value of θ should thus be essentially constant vs potential when the respective halogen evolution conditions proceed, and the reaction rate should be virtually independent of E or $[X^-]$ in case of the V-T mechanism. The reactions nonetheless behave as if θ is still low near the onset, which suggests that the pre-adsorbed species are not the actual reactants. This situation is very similar to the evolution of H_2 on Pt, which takes place while Pt is demonstrably saturated by H*, yet shows Tafel slopes of ~30 mV dec^{-1} at low overpotentials. To explain this disparity, the concept of "overpotential-deposited hydrogen"[70] has been invoked; a similar approach might be advisable for the BER and the CER. The apparent differences between the reactions is then perhaps due to differing interactions of overpotential-deposited Br* and Cl* with the emerging PtO_x layer. To better describe the CER, an approach that also includes a description of local interactions between adsorbed species may be needed, as has been done previously for competitive adsorption of Br^- and H^+ on Pt(100).[71] Use of a more complex isotherm (such as Frumkin) will probably not be more accurate as long as it still relies on the mean-field approximation, which cannot account for structured adlayers. In this regard, additional studies of halogen evolution on single crystal Pt surfaces could be very useful.

References

1. N. S. Lewis, "Toward cost-effective solar energy use." *Science*, **315**, 798 (2007).
2. I. Staffell, D. Scamman, A. Velazquez Abad, P. Balcombe, P. E. Dodds, P. Ekins, N. Shah, and K. R. Ward, "The role of hydrogen and fuel cells in the global energy system." *Energy Environ. Sci.*, **12**, 463 (2019).
3. O. Schmidt, A. Gambhir, I. Staffell, A. Hawkes, J. Nelson, and S. Few, "Future cost and performance of water electrolysis: an expert elicitation study." *Int. J. Hydrogen Energy*, **42**, 30470 (2017).
4. J. Bennett, "Electrodes for generation of hydrogen and oxygen from seawater." *Int. J. Hydrogen Energy*, **5**, 401 (1980).
5. S. Dresp, F. Dionigi, M. Klingenhof, and P. Strasser, "Direct Electrolytic Splitting of Seawater: Opportunities and Challenges." *ACS Energy Lett.*, **4**, 933 (2019).
6. K. Fujimura, K. Izumiya, A. Kawashima, E. Akiyama, H. Habazaki, N. Kumagai, and K. Hashimoto, "Anodically deposited manganese-molybdenum oxide anodes with high selectivity for evolving oxygen in electrolysis of seawater." *J. Appl. Electrochem.*, **29**, 765 (1999).
7. A. El-Moneim, N. Kumagai, K. Asami, and K. Hashimoto, "Nanocrystalline manganese-molybdenum-tungsten oxide anodes for oxygen evolution in acidic seawater electrolysis." *Mater. Trans.*, **46**, 309 (2005).
8. F. Dionigi, T. Reier, Z. Pawolek, M. Gliech, and P. Strasser, "Design criteria, operating conditions, and nickel-iron hydroxide catalyst materials for selective seawater electrolysis." *ChemSusChem.*, **9**, 962 (2016).
9. S. Trasatti, "Electrocatalysis in the anodic evolution of oxygen and chlorine." *Electrochim. Acta*, **29**, 1503 (1984).
10. J. E. Yourey, K. J. Pyper, J. B. Kurtz, and B. M. Bartlett, "Chemical stability of $CuWO_4$ for photoelectrochemical water oxidation." *J. Phys. Chem. C*, **117**, 8708 (2013).
11. V. Petrykin, K. M. Macounová, O. Shlyakhtin, and P. Krtil, "Tailoring the selectivity for electrocatalytic oxygen evolution on ruthenium oxides by zinc substitution." *Angew. Chemie - Int. Ed.*, **49**, 4813 (2010).
12. R. S. Magazinovic, B. C. Nicholson, D. E. Mulcahy, and D. E. Davey, "Bromide levels in natural waters: its relationship to levels of both chloride and total dissolved solids and the implications for water treatment." *Chemosphere*, **57**, 329 (2004).
13. S. Schulz and H. H. Hahn, "Generation of halogenated organic compounds in municipal waste water." *Water Sci. Technol.*, **37**, 303 (1998).
14. Y.-X. Sun, Q.-Y. Wu, H.-Y. Hu, and J. Tian, "Effect of bromide on the formation of disinfection by-products during wastewater chlorination." *Water Res.*, **43**, 2391 (2009).
15. C. Tian, R. Liu, T. Guo, H. Liu, Q. Luo, and J. Qu, "Chlorination and chloramination of high-bromide natural water: DBPs species transformation." *Sep. Purif. Technol.*, **102**, 86 (2013).
16. T. F. O'Brien, T. V. Bommaraju, and F. Hine, in *Handbook of Chlor-Alkali Technology* (Springer US, Boston, MA) Vol. 1 (2005).
17. R. K. B. Karlsson and A. Cornell, "Selectivity between oxygen and chlorine evolution in the chlor-alkali and chlorate processes." *Chem. Rev.*, **116**, 2982 (2016).
18. H. Yalçin, T. Koç, and V. Pamuk, "Hydrogen and bromine production from concentrated sea-water." *Int. J. Hydrogen Energy*, **22**, 967 (1997).
19. I. Cohen, B. Shapira, E. Avraham, A. Soffer, and D. Aurbach, "Bromide ions specific removal and recovery by electrochemical desalination." *Environ. Sci. Technol.*, **52**, 6275 (2018).
20. M. B. Heeb, J. Criquet, S. G. Zimmermann-Steffens, and U. von Gunten, "Oxidative treatment of bromide-containing waters: formation of bromine and its reactions with inorganic and organic compounds—a critical review." *Water Res.*, **48**, 15 (2014).
21. B. E. Conway and D. M. Novak, "Chloride ion adsorption effects in the recombination-controlled kinetics of anodic chlorine evolution at pt electrodes." *J. Chem. Soc. Faraday Trans. 1 Phys. Chem. Condens. Phases*, **75**, 2454 (1979).
22. B. E. Conway, Y. Phillips, and S. Y. Qian, "Surface electrochemistry and kinetics of anodic bromine formation at platinum." *J. Chem. Soc. Faraday Trans.*, **91**, 283 (1995).
23. J. A. Harrison and S. D. Hermijanto, "The oxidation of chloride ions and bromide ions on ruthenium dioxide electrodes." *J. Electroanal. Chem. Interfacial Electrochem.*, **225**, 159 (1987).
24. I. C. Man, *Theoretical Study of Electro-Catalysts for Oxygen Evolution*, Technical University of Denmark (2011).
25. J. Tymoczko, V. Colic, A. Ganassin, W. Schuhmann, and A. S. Bandarenka, "Influence of the alkali metal cations on the activity of Pt(111) towards model electrocatalytic reactions in acidic sulfuric media." *Catal. Today*, **244**, 96 (2015).
26. J. Suntivich, E. E. Perry, H. A. Gasteiger, and Y. Shao-Horn, "The influence of the cation on the oxygen reduction and evolution activities of oxide surfaces in alkaline electrolyte." *Electrocatalysis*, **4**, 49 (2013).
27. G. A. Ragoisha, T. A. Auchynnikava, E. A. Streltsov, and S. M. Rabchynski, "Electrochemical impedance of platinum in concentrated chloride solutions under potentiodynamic anodic polarization: effect of alkali metal cations." *Electrochim. Acta*, **122**, 218 (2014).
28. R. C. Beckwith, T. X. Wang, and D. W. Margerum, "Equilibrium and kinetics of bromine hydrolysis." *Inorg. Chem.*, **35**, 995 (1996).
29. Q. Liu and D. W. Margerum, "Equilibrium and kinetics of bromine chloride hydrolysis." *Environ. Sci. Technol.*, **35**, 1127 (2001).
30. J. G. Vos and M. T. M. Koper, "Measurement of competition between oxygen evolution and chlorine evolution using rotating ring-disk electrode voltammetry." *J. Electroanal. Chem.*, **819**, 260 (2018).
31. S. Trasatti, "Progress in the understanding of the mechanism of chlorine evolution at oxide electrodes." *Electrochim. Acta*, **32**, 369 (1987).
32. B. E. Conway and P. Gu, "Evaluation of Cl? adsorption in anodic Cl_2 evolution at Pt by means of impedance and potential-relaxation experiments. Influence of the state of surface oxidation of the Pt." *J. Chem. Soc. Faraday Trans.*, **87**, 2705 (1991).
33. E. Gileadi and G. E. Stoner, "The effect of competition with water on the kinetic parameters in electrode reactions." *J. Electrochem. Soc.*, **118**, 1316 (1971).
34. L. I. Krishtalik, "Kinetics and mechanism of anodic chlorine and oxygen evolution reactions on transition metal oxide electrodes." *Electrochim. Acta*, **26**, 329 (1981).
35. J. L. Fernández, M. R. Gennero de Chialvo, and A. C. Chialvo, "Analysis of the volmer–krishtalic mechanism for the chlorine electrode reaction." *Electrochem. Commun.*, **2**, 630 (2000).
36. B. V. Tilak and B. E. Conway, "Analytical relations between reaction order and tafel slope derivatives for electrocatalytic reactions involving chemisorbed intermediates." *Electrochim. Acta*, **37**, 51 (1992).
37. E. Gileadi, "The combined adsorption isotherm." *Electrochim. Acta*, **32**, 221 (1987).
38. E. Gileadi, "Problems in interfacial electrochemistry that have been swept under the carpet." *J. Solid State Electrochem.*, **15**, 1359 (2011).
39. B. E. Conway and G. Ping, "Surface electrochemistry of the anodic Cl_2 evolution reaction at Pt. influence of Co-deposition of surface oxide species on adsorption of the Cl intermediate." *J. Chem. Soc. Faraday Trans.*, **86**, 923 (1990).
40. B. E. Conway, "Method for kinetic analysis of a recombination-controlled reaction over a wide range of current-densities from the reversible region up to the limiting current." *J. Electrochem. Soc.*, **128**, 1022 (1981).
41. S. G. Roscoe and B. E. Conway, "State of surface oxide films at pt anodes and "volcano" behaviour in electrocatalysis for anodic Cl_2 evolution." *J. Electroanal. Chem.*, **224**, 163 (1987).
42. V. Consonni, S. Trasatti, F. H. Pollak, and W. E. O'Grady, "Mechanism of chlorine evolution on oxide anodes: study of PH effects." *J. Electroanal. Chem.*, **228**, 393 (1987).
43. W. D. Cooper and R. Parsons, "Kinetics of the bromine/bromide electrode on platinum in aqueous sulphuric acid." *Trans. Faraday Soc.*, **66**, 1698 (1970).
44. S. Ferro and A. De Battisti, "The bromine electrode. Part I: adsorption phenomena at polycrystalline platinum electrodes." *J. Appl. Electrochem.*, **34**, 981 (2004).
45. J. Xu, N. S. Georgescu, and D. A. Scherson, "The oxidation of bromide on platinum electrodes in aqueous acidic solutions: electrochemical and in situ spectroscopic studies." *J. Electrochem. Soc.*, **161**, H392 (2014).
46. G. Horányi and E. M. Rizmayer, "The problem of the irreversibility of the adsoprtion of halides on platinum." *J. Electroanal. Chem. Interfacial Electrochem.*, **83**, 367 (1977).
47. T. X. Wang, M. D. Kelley, J. N. Cooper, R. C. Beckwith, and D. W. Margerum, "Equilibrium, kinetic, and UV-spectral characteristics of aqueous bromine chloride, bromine, and chlorine species." *Inorg. Chem.*, **33**, 5872 (1994).
48. Y. Jung, E. Hong, Y. Yoon, M. Kwon, and J. Kang, "Formation of bromate and chlorate during ozonation and electrolysis in seawater for ballast water treatment." *Ozone Sci. Eng.*, **36**, 515 (2014).
49. N. M. Marković, H. A. Gasteiger, B. N. Grgur, and P. N. Ross, "Oxygen reduction reaction on Pt(111): effects of bromide." *J. Electroanal. Chem.*, **467**, 157 (1999).
50. B. E. Conway and D. M. Novak, "Electrocatalytic effect of the oxide film at pt anodes on Cl-recombination kinetics in chlorine evolution." *J. Electroanal. Chem. Interfacial Electrochem.*, **99**, 133 (1979).
51. S. Ferro, C. Orsan, and A. De Battisti, "The bromine electrode part II: reaction kinetics at polycrystalline Pt." *J. Appl. Electrochem.*, **35**, 273 (2005).

52. A. V. Sergeev, T. K. Zakharchenko, A. V. Chertovich, and D. M. Itkis, "Applying the deconvolution approach in order to enhance RRDE time resolution: experimental noise and imposed limitations." *Electrochim. Acta*, **298**, 858 (2019).
53. J. G. Vos and M. T. M. Koper, "Examination and prevention of ring collection failure during gas-evolving reactions on a rotating ring-disk electrode." *J. Electroanal. Chem.*, **850**, 113363 (2019).
54. P. Jovanovič, A. Pavlišič, V. S. Šelih, M. Šala, N. Hodnik, M. Bele, S. Hočevar, and M. Gaberšček, "New insight into platinum dissolution from nanoparticulate platinum-based electrocatalysts using highly sensitive in situ concentration measurements." *Chem. Cat. Chem.*, **6**, 449 (2014).
55. S. Geiger, S. Cherevko, and K. J. J. Mayrhofer, "Dissolution of platinum in presence of chloride traces." *Electrochim. Acta*, **179**, 24 (2015).
56. D. M. Novak and B. E. Conway, "Competitive adsorption and state of charge of halide ions in monolayer oxide film growth processes at Pt anodes." *J. Chem. Soc. Faraday Trans. 1 Phys. Chem. Condens. Phases*, **77**, 2341 (1981).
57. N. Garcia-Araez, V. Climent, E. Herrero, J. Feliu, and J. Lipkowski, "Thermodynamic studies of bromide adsorption at the Pt(111) electrode surface perchloric acid solutions: comparison with other anions." *J. Electroanal. Chem.*, **591**, 149 (2006).
58. A. Vacca, M. Mascia, S. Palmas, L. Mais, and S. Rizzardini, "On the formation of bromate and chlorate ions during electrolysis with boron doped diamond anode for seawater treatment." *J. Chem. Technol. Biotechnol.*, **88**, 2244 (2013).
59. C. M. A. Brett and A. M. O. Brett, in *Electrochemistry, Principles, Methods, and Applications., Oxford, 1993. 427s., Broschur 25.00 £. – ISBN* (Oxford University Press, Oxford) (1994).
60. G. Jerkiewicz, G. Vatankhah, J. Lessard, M. P. Soriaga, and Y.-S. Park, "Surface-oxide growth at platinum electrodes in aqueous H_2SO_4." *Electrochim. Acta*, **49**, 1451 (2004).
61. J. Xu and D. Scherson, "Quantitative in situ differential reflectance spectroscopy analysis of polycrystalline platinum oxidation in an aqueous acidic electrolyte." *ECS Electrochem. Lett.*, **4**, H46 (2015).
62. R. S. Patil, V. A. Juvekar, and V. M. Naik, "Oxidation of chloride ion on platinum electrode: dynamics of electrode passivation and its effect on oxidation kinetics." *Ind. Eng. Chem. Res.*, **50**, 12946 (2011).
63. M. T. M. Koper, A. P. J. Jansen, and J. J. Lukkien, "Lattice–gas modeling of electrochemical langmuir–hinshelwood surface reactions." *Electrochim. Acta*, **45**, 645 (1999).
64. N. M. Marković, C. A. Lucas, H. A. Gasteiger, and P. N. Ross, "Bromide adsorption on Pt(100): rotating ring-Pt(100) disk electrode and surface X-ray scattering measurements." *Surf. Sci.*, **365**, 229 (1996).
65. H. A. Gasteiger, N. M. Marković, and P. N. Ross, "Bromide adsorption on Pt(111): adsorption isotherm and electrosorption valency deduced from RRD Pt(111) E measurements." *Langmuir*, **12**, 1414 (1996).
66. J. Xu and D. Scherson, "Quantitative correlations between the normal incidence differential reflectance and the coverage of adsorbed bromide on a polycrystalline platinum rotating disk electrode." *Anal. Chem.*, **85**, 2795 (2013).
67. N. Garcia-Araez, V. Climent, E. Herrero, J. Feliu, and J. Lipkowski, "Thermodynamic studies of chloride adsorption at the Pt(111) electrode surface from 0.1 M $HClO_4$ solution." *J. Electroanal. Chem.*, **576**, 33 (2005).
68. D. J. Campbell, M. L. Lynch, and R. M. Corn, "Second harmonic generation studies of anionic chemisorption at polycrystalline platinum electrodes." *Langmuir*, **6**, 1656 (1990).
69. N. M. Marković and P. N. Ross, "The Effect of specific adsorption of ions and underpotential deposition of copper on the electro-oxidation of methanol on platinum single-crystal surfaces." *J. Electroanal. Chem.*, **330**, 499 (1992).
70. B. E. Conway and B. V. Tilak, "Interfacial processes involving electrocatalytic evolution and oxidation of H_2, and the role of chemisorbed H." *Electrochim. Acta*, **47**, 3571 (2002).
71. N. Garcia-Araez, J. J. Lukkien, M. T. M. Koper, and J. M. Feliu, "Competitive adsorption of hydrogen and bromide on Pt(100): mean-field approximation vs Monte Carlo simulations." *J. Electroanal. Chem.*, **588**, 1 (2006).